ISSN 1330–0016
CODEN FIZBE7

INVESTIGATION OF $\Lambda\Lambda$ DYNAMICS AND EFFECTIVE ΛN INTERACTION IN LOW AND MEDIUM MASS HYPERNUCLEI

MD. ABDUL KHAN and TAPAN KUMAR DAS

Department of Physics, University of Calcutta, 92, Acharya Prafulla Chandra Road, Calcutta - 700009, India

Received 14 October 2000; Accepted 26 February 2001

We critically review the $\Lambda\Lambda$ dynamics by examining Λ–Λ and Λ–nucleon phenomenological potentials in the study of the bound state properties of double-Λ hypernuclei ${}^{6}_{\Lambda\Lambda}$He, ${}^{10}_{\Lambda\Lambda}$Be, ${}^{14}_{\Lambda\Lambda}$C, ${}^{18}_{\Lambda\Lambda}$O, ${}^{22}_{\Lambda\Lambda}$Ne, ${}^{26}_{\Lambda\Lambda}$Mg, ${}^{30}_{\Lambda\Lambda}$Si, ${}^{34}_{\Lambda\Lambda}$S, ${}^{38}_{\Lambda\Lambda}$Ar, ${}^{42}_{\Lambda\Lambda}$Ca, ${}^{92}_{\Lambda\Lambda}$Zr and ${}^{142}_{\Lambda\Lambda}$Ce, ${}^{210}_{\Lambda\Lambda}$Pb in the framework of (core+Λ+Λ) three-body model. An effective ΛN potential is obtained by folding the phenomenological ΛN potential into the density distribution of core nuclei. The former two cases (i.e. ${}^{6}_{\Lambda\Lambda}$He and ${}^{10}_{\Lambda\Lambda}$Be) are revisited to justify the correctness of the present potential model. Assuming the same potential model, we predicted some of the structural properties of heavier double-Λ hypernuclei. The hyperspherical harmonics expansion method, which is an essentially exact method, has been employed for the three-body system. A convergence in binding energy up to 0.25% for $K_{\max} = 20$ has been achieved. In our calculation we have made no approximation in restricting the allowed l-values of the interacting pairs.

PACS numbers: 21.80.+a, 21.60.Jz, 21.30.Fe UDC 535.217, 539.21

Keywords: $\Lambda\Lambda$ dynamics, Λ–Λ and Λ–nucleon phenomenological potentials, double-Λ hypernuclei, ${}^{6}_{\Lambda\Lambda}$He, ${}^{10}_{\Lambda\Lambda}$Be, ${}^{14}_{\Lambda\Lambda}$C, ${}^{18}_{\Lambda\Lambda}$O, ${}^{22}_{\Lambda\Lambda}$Ne, ${}^{26}_{\Lambda\Lambda}$Mg, ${}^{30}_{\Lambda\Lambda}$Si, ${}^{34}_{\Lambda\Lambda}$S, ${}^{38}_{\Lambda\Lambda}$Ar, ${}^{42}_{\Lambda\Lambda}$Ca, ${}^{92}_{\Lambda\Lambda}$Zr, ${}^{142}_{\Lambda\Lambda}$Ce, ${}^{210}_{\Lambda\Lambda}$Pb, (core+$\Lambda$+$\Lambda$) three-body model, hyperspherical harmonics expansion method

1. Introduction

The study of the structure of light exotic hypernuclei has become an area of particular interest since the discovery of this species in the early sixties [1-3]. Important members of this new species are the nuclei ${}^{5}_{\Lambda}$He, ${}^{9}_{\Lambda}$Be, ${}^{13}_{\Lambda}$C, ${}^{6}_{\Lambda\Lambda}$He, ${}^{10}_{\Lambda\Lambda}$Be and ${}^{13}_{\Lambda\Lambda}$B [1-8]. Discovery of these double-Λ hypernuclei opened a new avenue to extract important informations about the $\Lambda\Lambda$ interaction. Again, since hyperons as well as nucleons both have qqq structure (e.g., p$\rightarrow$ uud, n$\rightarrow$ udd, $\Lambda^0 \rightarrow$ uds etc., where u, d and s are up, down and strange quarks, respectively), the interaction among them as well as with nucleons should give important inputs in the knowledge of strong (qq) interactions. That in turn enhances the range of ones imagination on possible existence of multistrange hypernuclei and derivation of true hyperon-hyperon and hyperon-nucleon interactions. In the early stages, the emulsion experiments provided a source of information on hypernuclei, which was limited to binding energies of Λ-particle in the light hypernuclei and the decay rates (life times) [2]. The binding energy data provided physicists with some qualitative informations about the Λ–nucleon (ΛN) interaction and single-particle potential strength for Λ-particle in hypernuclei [9]. The hyperon nucleon scattering experiments have also been performed but they are still in primary stages and do not provide detailed phase shifts to construct the potential reliably. Some Λ–N and Σ–N total cross-sections and very few angular distribution at low energies have been measured [10-15], but they are not sufficient to allow the phase-shift analysis. Nevertheless, the bound-state properties of single-Λ and double-Λ hypernuclei can give valuable indirect information about ΛN and $\Lambda\Lambda$ interactions. One can, for example, take phenomenological forms of ΛN and $\Lambda\Lambda$ interactions and see if they reproduce the observables of the hypernuclei. Alternatively, one can adjust the parameters of the empirical potential to reproduce the bound state properties and thus predict the effective ΛN and $\Lambda\Lambda$ interactions. Earlier attempts in this direction [16-20] used variational and approximate few-body calculations for the hypernucleus treated as a few-body system.

In the present work, we test our potential model (i.e., the $\Lambda\Lambda$ and the effective ΛN potential which we obtained by folding the phenomenological ΛN potential into the density distribution of the core nuclei) by studying the general state properties of double-Λ hypernuclei ${}^{6}_{\Lambda\Lambda}$He and ${}^{10}_{\Lambda\Lambda}$Be for which the ground state binding energy is known experimentally. We then apply our potential model to investigate the ground state structural properties of double-Λ hypernuclei ${}^{14}_{\Lambda\Lambda}$C, ${}^{18}_{\Lambda\Lambda}$O, ${}^{22}_{\Lambda\Lambda}$Ne, ${}^{26}_{\Lambda\Lambda}$Mg, ${}^{30}_{\Lambda\Lambda}$Si, ${}^{34}_{\Lambda\Lambda}$S, ${}^{38}_{\Lambda\Lambda}$Ar, ${}^{42}_{\Lambda\Lambda}$Ca, ${}^{92}_{\Lambda\Lambda}$Zr, ${}^{142}_{\Lambda\Lambda}$Ce and ${}^{210}_{\Lambda\Lambda}$Pb (for which the experimental data are not available) treating them as core+Λ+Λ three-body system. (No $\Lambda\Lambda$ bound state has been reported). We employ hyperspherical harmonics expansion (HHE) method to solve such a three-body system. This method is a powerful tool for the *ab initio* solution of the few-body Schrödinger equation for a given set of interaction potentials among the constituent particles. This method has been used for bound states in atomic [21-38], nuclear [39-50] and particle physics [51-53]. Attempts have been made to use it in scattering problems as well [54]. In this method, the wave function is expanded in a complete set of hyperspherical harmonics (HH), which are, for a three-body system, the six-dimensional analogue of ordinary spherical harmonics, which are the angular part of eigenfunctions of 3-dimensional Laplacian operator. The resulting Schrödinger equation is a set of coupled differential equations which are solved numerically by the renormalized Numerov method (RNM) [55-56]. The HHE method is essentially an exact one and more reliable than other methods. It involves no approximation other than an eventual truncation of the expansion basis. By gradually expanding the expansion basis and checking the rate of convergence, any desired precision in the binding energy can, in principle, be achieved. However, the number of coupled differential equations and, therefore, the complexity in the numerical solution increases rapidly as the expansion basis is increased by including larger hyperangular-momentum quantum numbers. Computer limitations set an ultimate limit to the precision attainable. Thus in this approach, the attainment of desired convergence in physical observables are of great importance.

In the present calculation, we achieved a convergence in the binding energy to within 0.25%. In addition to the two-Λ separation energy ($B_{\Lambda\Lambda}$) and $\Lambda\Lambda$ bond energy ($\Delta B_{\Lambda\Lambda}$), which are defined as

$$B_{\Lambda\Lambda}({}^{A}_{\Lambda\Lambda}Z) = [M({}^{A-2}Z) + 2M_{\Lambda} - M({}^{A}_{\Lambda\Lambda}Z)]c^2 \tag{1}$$

and

$$\Delta B_{\Lambda\Lambda} = B_{\Lambda\Lambda}({}^{A}_{\Lambda\Lambda}Z) - 2B_{\Lambda}({}^{A-1}_{\Lambda}Z)\,, \tag{2}$$

we have also studied the size, density distribution and correlation among the core and the valence Λ-hyperons.

This paper is organized as follows: In Sect. 2, we review the HHE method for a three-body system consisting of non-identical particles. Results of calculation and discussion are presented in Sect. 3. Finally, in Sect. 4 we draw our conclusions.

2. HHE method

We label the core as particle no '1' and the two valence Λ-particles as particles '2' and '3', respectively (see Fig. 1). For pairwise interactions, we can treat any one of the three particles as the spectator, remaining two being the interacting pair. Thus there are three possible partitions labelled 'i' (i=1, 2, 3). In the partition 'i', particle numbered 'i' is the spectator and particles numbered 'j' and 'k' form the interacting pair ($i, j, k = 1, 2, 3$, cyclic). Now, for a given partition 'i', the Jacobi coordinates (which are proportional to the relative separation between the interacting

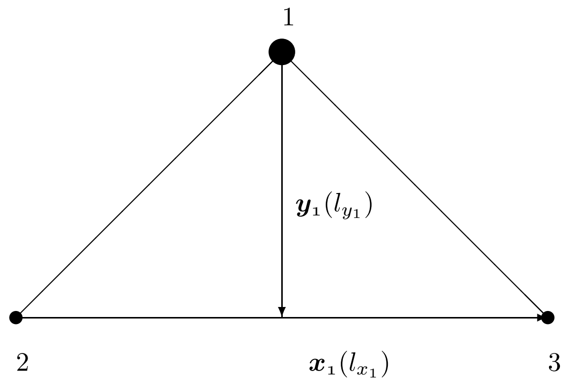

Fig. 1. Choice of Jacobi coordinates for the partition '1'.

pair and the relative separation between the spectator and the centre of mass of the interacting pair, respectively) are defined as

$$\begin{aligned} \boldsymbol{x}_i &= a_{jk}(\boldsymbol{r}_j - \boldsymbol{r}_k)\,, \\ \boldsymbol{y}_i &= a_{(jk)i}\left(\boldsymbol{r}_i - \frac{m_j\boldsymbol{r}_j + m_k\boldsymbol{r}_k}{m_j + m_k}\right), \\ \boldsymbol{R} &= \frac{1}{M}\left(m_i\boldsymbol{r}_i + m_j\boldsymbol{r}_j + m_k\boldsymbol{r}_k\right). \end{aligned} \tag{3}$$

The coefficients a_{jk} and $a_{(jk)i}$ are defined as $a_{jk} = \left[m_j m_k M/\{m_i(m_j+m_k)^2\}\right]^{1/4}$ and $a_{(jk)i} = \left[m_i(m_j+m_k)^2/\{m_j m_k M\}\right]^{1/4}$ (i, j, k=1, 2, 3 cyclic), where m_i, $\boldsymbol{r}_i$ are the mass and position of the $i^{\rm th}$ particle, $M = m_i + m_j + m_k$ is the total mass and $\boldsymbol{R}$ is the centre of mass of the system. The sign of $\boldsymbol{x}_i$ is fixed by the condition that 'i', 'j', 'k' form a cyclic permutation of (1, 2, 3). In the transformation (2), the six dimensional volume element is conserved (i.e., the Jacobian is unity) and the centre of mass motion is automatically separated. The relative motion of the three-body system is described by the Schrödinger equation

$$\left[-\frac{\hbar^2}{2\mu}(\nabla^2_{x_i} + \nabla^2_{y_i}) + V_{jk}(\boldsymbol{x}_i) + V_{ki}(\boldsymbol{x}_i, \boldsymbol{y}_i) + V_{ij}(\boldsymbol{x}_i, \boldsymbol{y}_i) - E\right]\Psi(\boldsymbol{x}_i, \boldsymbol{y}_i) = 0 \tag{4}$$

where $\mu = \left[m_i m_j m_k/M\right]^{1/2}$ is an effective-mass parameter and V_{ij} is the interaction potential between $i^{\rm th}$ and $j^{\rm th}$ particles. We next introduce the hyperspherical variables defined by [50]

$$\begin{aligned} x_i &= \rho\cos\phi_i \\ y_i &= \rho\sin\phi_i\,, \end{aligned} \tag{5}$$

where $\rho = \sqrt{x_i^2 + y_i^2}$ is the global length (also called the hyper-radius), which is invariant under the three-dimensional rotations and permutations of the particle indices. Thus, ρ is the same for all three partitions. The five other hyperspherical variables include the hyperspherical angle $\phi_i = \tan^{-1}(y_i/x_i)$ and the polar angles $(\theta_{x_i}, \phi_{x_i})$ and $(\theta_{y_i}, \phi_{y_i})$ giving orientations of $\boldsymbol{x}_i$ and $\boldsymbol{y}_i$, respectively. These are collectively denoted by

$$\Omega_i \equiv \{\phi_i, \theta_{x_i}, \phi_{x_i}, \theta_{y_i}, \phi_{y_i}\} \tag{6}$$

and are called the "hyperangles". The six-dimensional volume element is given by

$$dV_6 = \rho^5\ {\rm d}\rho\ \cos^2\phi_i\ \sin^2\phi_i\ {\rm d}\phi_i {\rm d}\Omega_{x_i}{\rm d}\Omega_{y_i}\,, \tag{7}$$

where

$$\begin{aligned} d\Omega_{x_i} &= sin\theta_{x_i}\ d\theta_{x_i}\ d\phi_{x_i} \\ d\Omega_{y_i} &= sin\theta_{y_i}\ d\theta_{y_i}\ d\phi_{y_i}\,. \end{aligned} \tag{8}$$

In terms of the hyperspherical variables, the Schrödinger equation becomes

$$\left[-\frac{\hbar^2}{2\mu}\{\frac{1}{\rho^5}\frac{\partial}{\partial\rho}(\rho^5\frac{\partial}{\partial\rho})-\frac{\hat{\mathcal{K}}^2(\Omega_i)}{\rho^2}\}+V(\rho,\Omega_i)-E\right]\Psi(\rho,\Omega_i) \;=\; 0\,, \tag{9}$$

where $V(\rho,\Omega_i)=V_{jk}(\boldsymbol{x}_i)+V_{ki}(\boldsymbol{x}_i,\boldsymbol{y}_i)+V_{ij}(\boldsymbol{x}_i,\boldsymbol{y}_i)$ is the total interaction potential expressed in terms of the hyperspherical variables, and $\hat{\mathcal{K}}^2(\Omega_i)$ is the square of the hyperangular-momentum operator given by [50]

$$\hat{\mathcal{K}}^2(\Omega_i) \;=\; -\frac{\partial^2}{\partial{\phi_i}^2}-4\cot 2\phi_i\;\frac{\partial}{\partial\phi_i}+\frac{1}{\cos^2\phi_i}\hat{l}^2(\hat{x_i})+\frac{1}{\sin^2\phi_i}\hat{l}^2(\hat{y_i}), \tag{10}$$

where $\hat{l}^2(\hat{x_i})$ and $\hat{l}^2(\hat{y_i})$ are the squares of ordinary orbital angular-momentum operators associated with $\boldsymbol{x}_i$ and $\boldsymbol{y}_i$ motions. The operator $\hat{\mathcal{K}}^2$ satisfies the eigenvalue equation [50]

$$\hat{\mathcal{K}}^2(\Omega_i)\mathcal{Y}_{K\alpha_i}(\Omega_i) \;=\; K(K+4)\mathcal{Y}_{K\alpha_i}(\Omega_i)\,, \tag{11}$$

where α_i is an abbreviation for the set of four quantum numbers $\{l_{x_i},l_{y_i},L,M\}$ and K, the hyperangular-momentum quantum number (which is not a conserved quantity for the three-body system) is given by $K=2n_i+l_{x_i}+l_{y_i}$ (n_i being a non-negative integer). The number K is the degree of the homogeneous harmonic polynomials $\rho^K\mathcal{Y}_{K\alpha_i}(\Omega_i)$ in the Cartesian components of $\boldsymbol{x}_i$ and $\boldsymbol{y}_i$. Note that the quantum number K is invariant under the change of partition and hence does not involve the partition label. The eigenfunctions of $\hat{\mathcal{K}}^2$ are called hyperspherical harmonics (HH) and are given by

$$\mathcal{Y}_{K\alpha_i}(\Omega_i)={}^{(2)}P_K{}^{l_{y_i}\,l_{x_i}}(\phi_i)\left[Y_{l_{x_i}}(\hat{x_i})\;Y_{l_{y_i}}(\hat{y_i})\right]_{LM}, \tag{12}$$

where

$${}^{(2)}P_K{}^{l_{y_i}\,l_{x_i}}(\phi_i)=N_K{}^{l_{x_i},l_{y_i}}(\cos\;\phi_i)^{l_{x_i}}\;(\sin\;\phi_i)^{l_{y_i}}P_{n_i}{}^{l_{y_i}+1/2,l_{x_i}+1/2}\;(\cos\;2\phi_i)\,. \tag{13}$$

The normalization constant $N_K^{l_{x_i},l_{y_i}}$ is given by

$$N_K^{l_{x_i},L_{y_i}} \;=\; \left[\frac{2\;n_i!\;(K+2)(n_i\;+\;l_{x_i}\;+\;l_{y_i}\;+\;1)!}{\Gamma(n_i\;+\;l_{x_i}\;+\;3/2)\;\Gamma(n_i\;+\;l_{y_i}+3/2)}\right]^{\frac{1}{2}} \tag{14}$$

and $P_n^{\alpha,\beta}(x)$ is the Jacobi polynomial [57]. The HH's $\{\mathcal{Y}_{K\alpha_i}(\Omega_i)\}$ form a complete orthonormal set in the angular hyperspace (Ω_i).

In the present method, the wave function $\Psi(\rho,\Omega_i)$ is expanded in the complete set of HH corresponding to a given partition (say partition 'i')

$$\Psi(\rho,\Omega_i)=\sum_{K\alpha_i}\frac{U_{K\alpha_i}(\rho)}{\rho^{5/2}}\mathcal{Y}_{K\alpha_i}(\Omega_i). \tag{15}$$

The factor $\rho^{-5/2}$ is included in order to remove the first-order derivative with respect to ρ in Eq. (9). Substitution of Eq. (15) in Eq. (9) and the use of the orthonormality of HH leads to a set of coupled differential equations (CDE) in ρ

$$\begin{aligned}&\left[-\frac{\hbar^2}{2\mu}\left(\frac{\mathrm{d}^2}{\mathrm{d}\rho^2}-\frac{\mathcal{L}_K(\mathcal{L}_K+1)}{\rho^2}\right)-E\right]U_{K\alpha_i}(\rho)\\&+\textstyle\sum_{K'\alpha_i{}'} < K\alpha_i \mid V(\rho,\Omega_i) \mid K'\alpha_i{}' > U_{K'\alpha_i{}'}(\rho) \;=\; 0,\end{aligned} \tag{16}$$

where $\mathcal{L}_K = K + 3/2$ and

$$< K\alpha_i|V(\rho,\Omega_i)|K'\alpha_i' > = \int\limits_{\Omega_i} \mathcal{Y}^*_{K\alpha_i}(\Omega_i)V(\rho,\Omega_i)\mathcal{Y}_{K'\alpha_i'}(\Omega_i)\mathrm{d}\Omega_i. \tag{17}$$

Since the expansion (15) is, in principle, an infinite one, the CDE, Eq. (16), are also an infinite set. For practical purposes, the expansion (15) has to be truncated to a finite set, leading to a finite set of CDE. Restrictions arising out of symmetry requirement and imposition of conserved quantum numbers (e.g., total angular momentum, parity etc.) can reduce the expansion basis further and consequently a smaller set of CDE is to be solved.

Evaluation of the matrix elements of the type $< \mathcal{Y}_{K\alpha_i}(\Omega_i)|V_{jk}(x_i)|\mathcal{Y}_{K'\alpha_i'}(\Omega_i) >$ (for central interactions) is straightforward, while those for the matrix elements of the type $< \mathcal{Y}_{K\alpha_i}(\Omega_i)|V_{ki}(x_j)|\mathcal{Y}_{K'\alpha_i'}(\Omega_i) >$ and $< \mathcal{Y}_{K\alpha_i}(\Omega_i)|V_{ij}(x_k)|\mathcal{Y}_{K'\alpha_i'}(\Omega_i) >$ become very complicated even for central interactions, since both $\boldsymbol{x}_j$ or $\boldsymbol{x}_k$ are expressed as linear combinations of $\boldsymbol{x}_i$ and $\boldsymbol{y}_i$, hence $\boldsymbol{x}_j$ and $\boldsymbol{x}_k$ depend on the polar angles of $\boldsymbol{x}_i$ and $\boldsymbol{y}_i$ (i.e. $\hat{x_i}$, $\hat{y_i}$) (see Eq. (2)). But the calculation of these matrix elements will be quite simple in the partitions 'j' or 'k', respectively, since in these partitions $\boldsymbol{x}_j$ or $\boldsymbol{x}_k$ are independent of $\boldsymbol{y}_j$ and $\boldsymbol{y}_k$, respectively. Since the choice of a particular partition is arbitrary, the HH basis corresponding to any chosen partition 'i' forms a complete set spanning the same hyperangular space. One can then relate the HH basis for two different partitions 'i' and 'j' through a unitary transformation. Then a particular element, $\mathcal{Y}_{K\alpha_i}(\Omega_i)$, in the partition '$i$' can be expanded in the HH basis corresponding to partition 'j' as

$$\mathcal{Y}_{K\alpha_i}(\Omega_i) \;=\; \sum_{l_{x_j} l_{y_j}} < l_{x_i} l_{y_i} \mid l_{x_j} l_{y_j} >_{KL} \mathcal{Y}_{K\alpha_j}(\Omega_j), \tag{18}$$

where the transformation coefficients $< l_{x_i} l_{y_i} \mid l_{x_j} l_{y_j} >_{KL}$ are called the Raynal Revai coefficients (RRC) [58]. Since K, L and M are independent of the partition, the sum is over l_{x_j} and l_{y_j} only, subject to the restrictions $\boldsymbol{l}_{x_i} + \boldsymbol{l}_{y_i} = \boldsymbol{L} = \boldsymbol{l}_{x_j} + \boldsymbol{l}_{y_j}$. These coefficients can be computed easily [38]. Since the RRC's do not involve 'ρ', they are calculated once only and stored. That reduces the CPU time significantly.

In terms of the RRC's, the matrix elements of V_{ki} in the partition 'i' can be writen as

$$\begin{aligned}\langle \mathcal{Y}_{K\alpha_i}(\Omega_i)|V_{ki}(x_j)|\mathcal{Y}_{K'\alpha_i{}'}(\Omega_i)\rangle &= \textstyle\sum_{l'_{x_j}l'_{y_j}l_{x_j}l_{y_j}} < l_{x_i}l_{y_i}|l_{x_j}l_{y_j} >^*_{KL} \\ &\times\ < l'_{x_i}l'_{y_i} \mid l'_{x_j}l'_{y_j} >_{K'L} \\ &\times\ \langle \mathcal{Y}_{K\alpha_j}(\Omega_j)|V_{ki}(x_j)|\mathcal{Y}_{K'\alpha'_j}(\Omega_j)\rangle.\end{aligned} \tag{19}$$

The matrix element on the right side of Eq. (19) has the same form as the matrix element of V_{jk} in the partition 'i' (preferred partition) and can be evaluated in a simple way. Thus by computing the RRC's involved in Eq. (19), the matrix element of V_{ki} in the partition 'i' can be evaluated easily. Similar technique can be employed for the calculation of the matrix element of V_{ij}.

Calculation of the potential matrix elements in the preferred partition (in which the pair interaction potential is a function only of the corresponding $\boldsymbol{x}$ of the partition) can be further simplified by introducing a multipolar expansion [39] of the potential. For a matrix element in the preferred partition, say partition 'i', the potential $V_{jk}(x_i)$, is expanded in an appropriate subset of corresponding HH

$$V_{jk}(x_i) = \sum_{K''\alpha''} v^{(jk)}_{K''\alpha''}(\rho)\mathcal{Y}_{K''\alpha''}(\Omega_i)\,, \tag{20}$$

where $v^{(jk)}_{K''\alpha''}(\rho)$ is called the potential multipole and can be evaluated by the use of the orthonormality of HH

$$v^{(jk)}_{K''\alpha''_i}(\rho) = \int V_{jk}(x_i)\mathcal{Y}^*_{K''\alpha''_i}(\Omega_i)\mathrm{d}\Omega_i. \tag{21}$$

The matrix element thus becomes

$$< \mathcal{Y}_{K\alpha_i}(\Omega_i)|V_{jk}(x_i)|\mathcal{Y}_{K'\alpha'_i}(\Omega_i) >= \sum_{K''\alpha''_i} v^{(jk)}_{K''\alpha''_i}(\rho) < K\alpha_i|K''\alpha''_i|K'\alpha'_i > \tag{22}$$

where

$$< K\alpha_i \mid K''\alpha''_i \mid K'\alpha'_i >= \int \mathcal{Y}^*_{K\alpha_i}(\Omega_i)\mathcal{Y}_{K''\alpha''_i}(\Omega_i)\mathcal{Y}_{K'\alpha'_i}(\Omega_i)\mathrm{d}\Omega_i \tag{23}$$

are called the geometrical structure coefficients (GSC). They are independent of ρ and the interaction. Hence, these coefficients need to be calculated once only and stored, resulting in a fast and efficient algorithm. The GSC's involved in Eq. (22) can be calculated by the standard numerical integration. However, they can be calculated in a very elegant manner [59] by using the completeness property of the HH basis. Finally, the set of CDE's, Eq. (16), is to be solved numericaly subject to appropriate boundary conditions to get the energy E and the partial waves $U_{K\alpha_i}(\rho)$.

3. Results and discussion

In the present calculation we have taken the core to be structureless. Since the core (^{4}He, ^{8}Be, ^{12}C, ^{16}O, ^{20}Ne, ^{24}Mg, ^{28}Si, ^{32}S, ^{36}Ar, ^{40}Ca, ^{90}Zr, ^{140}Ce or ^{208}Pb) contains only nucleons and no Λ-particles, there are no symmetry requirements under exchange of the valence Λ-particles with the core nucleons. The only symmetry requirements are (i) antisymmetrization of the core wave function under the exchange of the nucleons and (ii) antisymmetrization of the three-body wave function under exchange of the two Λ-particles. The former is implicitly taken care of in the choice of the core as a building block. The latter is correctly incorporated by restricting the l_{x_1} values, as discussed in detail in the following. Thus, within the three-body model, the symmetry requirements are correctly satisfied without the use any approximation. The ground state of all experimentally known double-Λ hypernuclei have a total angular momentum $J = 0$ and positive parity. We assume this to be true for all double-Λ hypernuclei with cores having $N = Z =$ even. The possible total spin (S) of the three-body system (core+Λ+Λ) can take two values 0 or 1 since the spin of the core in all the above cases is equal 0. Thus the total orbital angular momentum L can be either 0 or 1, corresponding to $S = 0$ or 1, respectively. Hence, the ground state of all the above double-Λ hypernuclei is an admixture of the states ^{1}S$_0$ and ^{3}P$_0$. Since the core is spinless, the spin singlet state ($S = 0$) corresponds to the zero total spin of the valence Λ-particles (i.e. $S_{23} = 0$). Hence the spin part of the wave function is antisymmetric under the exchange of the spins of the two Λ-particles. Thus the spatial part must be symmetric under the exchange of the two Λ-hyperons. The symmetry of the spatial part is determined by the hyperspherical harmonics, since the hyper-radius ρ and hence the hyper-radial partial waves ($U_{K\alpha}(\rho)$) are invariant under the permutation of the particles. Under the pair exchange operator P_{23}, which interchanges particles 2 and 3, $\boldsymbol{x}_1 \to -\boldsymbol{x}_1$ and $\boldsymbol{y}_1$ remains unchanged (see Eq. (2)). Consequently, P_{23} acts like the parity operator for the pair (23) only. Choosing the two valence Λ-hyperons to be in spin singlet state (spin antisymmetric), the space wave function must be symmetric under P_{23}. This then requires l_{x_1} to be even. For the spin singlet state, the total orbital angular momentum is $L = 0$, hence we must have $l_{x_1} = l_{y_1} =$ even integer. Since $K = 2n_1 + l_{x_1} + l_{y_1}$, where n_1 is a non-negative integer, K must be even and

$$
\begin{aligned}
l_{x_1} \quad = \quad l_{y_1} \quad &= \quad 0, 2, 4, ..., K/2 \qquad\qquad \text{if } K/2 \text{ is even} \\
&= \quad 0, 2, 4, ..., (K/2 - 1) \qquad \text{if } K/2 \text{ is odd}\,.
\end{aligned}
\tag{24}
$$

Again, for the triplet state ($S = 1$), the two valence Λ-hyperons will be in the spin triplet state ($S_{23} = 1$, spin symmetric). Hence the space wave function must be antisymmetric under P_{23}. This then requires l_{x_1} to be odd. For the spin triplet state, the total orbital angular momentum $L = 1$, hence l_{y_1} may take values l_{x_1} and $l_{x_1} \pm 1$, but the parity conservation allows $l_{y_1} = l_{x_1}$ only. Since $K = 2n_1 + l_{x_1} + l_{y_1}$, where n_1 is a non-negative integer, K must be even and

$$\begin{aligned} l_{x_1} = l_{y_1} &= 1,3,5,....,K/2 && \text{if } K/2 \text{ is odd} \\ &= 1,3,5,....,(K/2-1) && \text{if } K/2 \text{ is even}. \end{aligned} \tag{25}$$

For a practical calculation, the HH expansion basis (Eq. (15)) is truncated to a maximum value ($K_{\max}$) of K. For each allowed $K \leq K_{\max}$ with K=even integers, all allowed values of l_{x_1} (=0,1,2,3,4,.....,$K/2$) are included (if tensor forces are considered). The even l_{x_1} values correspond to $L = 0$, $S = 0$ and the odd l_{x_1} values correspond to $L = 1$, $S = 1$. This truncates Eq. (16) to a set of N coupled differential equations, where

$$\begin{aligned} N &= \left(\tfrac{1}{2}K_{\max}+1\right)\left(\tfrac{1}{4}K_{\max}+1\right) && \text{if } K/2 \text{ is even} \\ &= \left(\tfrac{1}{4}K_{\max}+2\right)\left(\tfrac{1}{2}K_{\max}+2\right) && \text{if } K/2 \text{ is odd}. \end{aligned} \tag{26}$$

The truncated set of CDE has been solved by the hyperspherical adiabatic approximation (HAA) [60].

3.1. Two-body potentials

A number of phenomenological as well as meson-exchange motivated forms were used for the ΛΛ interaction in earlier attempts. Based on the available data, some selection was made between Nijmegen potential models [61-62]. Since knowledge of ΛΛ scattering is still quite inadequate, it is not possible to establish realistic ΛΛ potentials at this stage. Instead, we adopt here a purely phenomenological strategy. We used the three-term Gaussian ΛΛ potential model D proposed by the Nijmegen group [63]. They proposed OBE potential models D and F based on the NN, ΛN and ΣN data along with the SU(3) symmetry. The Nijmegen D ΛΛ potential given by Refs. [61] and [62]

$$V_{\Lambda\Lambda}(r) = \sum_{i=1}^{3} V_i \exp(-\frac{r^2}{\beta_i^2}) \tag{27}$$

without any restriction over l values. The parameters of the ΛΛ interaction are listed in Table 1. The core–Λ potential is obtained by folding phenomenological Λ-nucleon potential (assumed one-term Gaussian) into the nuclear density distribution of the

Table 1. Parameters of ΛΛ interaction from Refs. [61] and [62]. (ND stands for Nijmegen potential D.)

i	1	2	3
β_i (fm)	1.5	0.9	0.5
V_i (ND)	-8.967	-226.800	880.700

core which is chosen to have an Wood-Saxon shape given by

$$\rho(r) = \frac{\rho_0}{1 + \exp(\frac{r-c}{a})} \tag{28}$$

with $c = r_0 A_c^{1/3}$ fm, $a = 0.60$ fm, $r_0 = 1.1$ fm (where c is termed the half density radius and a the skin thickness), and the density constant ρ_0 is determined by the condition

$$\int \rho(r) \mathrm{d}^3 r = A_c, \tag{29}$$

where A_c is the mass of the core in units of nucleon mass. The values of a and r_0 are chosen following suggestions in the literatutre [6,8]. The phenomenological ΛN potential is given by

$$V_{\Lambda N}(r) = V_0 \exp(-r^2/\chi^2) \tag{30}$$

with V_0 adjusted to reproduce the Λ binding energy (B_Λ) (experimental or empirical, see Table 2) in the core–Λ subsystem and $\chi = 1.034$ fm. Then the core-Λ potential is given by

$$V_{c\Lambda}(r) = \int \rho(r_1) V_{\Lambda N}(|\boldsymbol{r}_1 - \boldsymbol{r}|) \mathrm{d}^3 r_1. \tag{31}$$

The strength of ΛN potential is expected to be weakened with the increase in mass of the core due to the screening or shielding effect by neighbouring nucleons within

Table 2. Parameters of the ΛN potential and corresponding Λ separation energy in different ${}^{A-1}_{\Lambda}Z$ (i.e. core-Λ subsystems).

System	ΛN potential parameters		B_Λ (MeV)		
	V_0 (MeV)	χ (fm)	Experimental	Empirical	Calculated
${}^{5}_{\Lambda}$He	-71.05	1.034	3.12 ± 0.02 [9]	–	3.1214
${}^{9}_{\Lambda}$Be	-52.04	1.034	6.71 ± 0.04 [9]	–	6.7136
${}^{13}_{\Lambda}$C	-50.32	1.034	11.22 ± 0.08 [71]	–	11.2226
${}^{17}_{\Lambda}$O	-48.88	1.034	–	14.61 ± 1.5	14.6000
${}^{21}_{\Lambda}$Ne	-45.95	1.034	–	16.24 ± 1.5	16.2401
${}^{25}_{\Lambda}$Mg	-43.67	1.034	–	17.42 ± 1.5	17.4237
${}^{29}_{\Lambda}$Si	-41.88	1.034	–	18.32 ± 1.5	18.3322
${}^{33}_{\Lambda}$S	-40.41	1.034	–	19.04 ± 1.5	19.0440
${}^{37}_{\Lambda}$Ar	-39.21	1.034	–	19.62 ± 1.5	19.6224
${}^{41}_{\Lambda}$Ca	-38.19	1.034	–	20.11 ± 1.5	20.1158
${}^{91}_{\Lambda}$Zr	-31.35	1.034	22.10 ± 0.30 [62]	–	22.1668
${}^{141}_{\Lambda}$Ce	-30.73	1.034	24.50 ± 1.00 [62]	–	24.5028
${}^{209}_{\Lambda}$Pb	-30.62	1.034	26.30 ± 0.50 [62]	–	26.3107

the core when the interacting nucleon is embedded in the core. The π-mesic decay of Λ-hyperon ($\Lambda \rightarrow N + \pi$) is predominant in free space but tends to be suppressed in hypernucleus by the Pauli-exclusion principle and instead non-mesic weak process ($\Lambda + N \rightarrow N + N$) becomes dominant with increasing mass number [64-69]. Thus we actually get an effective ΛN interaction by the folding process. The parameters of this effective ΛN potential are listed in Table 2. A plot of effective ΛN potential strength against mass of the core is shown in Fig. 2. As evident from Eq. (26),

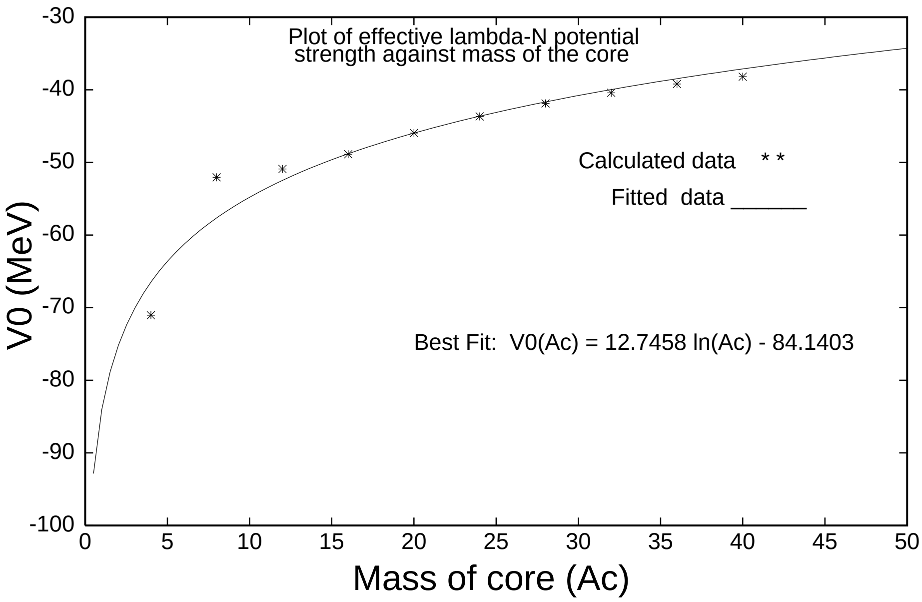

Fig. 2. Plot of the strength (V_0) of ΛN effective potential against mass of the core A_c. (Data taken from Table 2).

the number of basis states and hence the size of CDE increases rapidly as $K_{\max}$ increases. The truncated set of CDE takes the form

$$\left[-\frac{\hbar^2}{2\mu}\left(\frac{\mathrm{d}^2}{\mathrm{d}\rho^2} - \frac{\mathcal{L}_K(\mathcal{L}_K+1)}{\rho^2}\right) - E\right] U_{Kl_{x_1}LS}(\rho)$$
$$+ \sum_{K'=0,2,..}^{K_{\max}} \sum_{l'_{x_1}(\mathrm{allowed})} \sum_{(L'S')=(0,0),(1,1)} \langle K l_{x_1} | V(\rho,\Omega_1) | K' l'_{x_1} \rangle U_{K' l'_{x_1} L' S'}(\rho) = 0 \tag{32}$$

(allowed $l'_{x_1} = 0, 2, ...$ only for $S = 0, L = 0$, otherwise $l'_{x_1} = 1, 3, ...$ for $S = 1, L = 1$). Note that the subscripts l_{y_1} ($=l_{x_1}$) or l'_{y_1} ($=l'_{x_1}$) have been suppressed for brevity.

The calculated values of binding energy (BE), ΛΛ bond energy ($\Delta B_{\Lambda\Lambda}$) for $K_{\max} = 20$ for the ground states of ${}^{6}_{\Lambda\Lambda}$He, ${}^{10}_{\Lambda\Lambda}$Be, ${}^{14}_{\Lambda\Lambda}$C, ${}^{18}_{\Lambda\Lambda}$O, ${}^{22}_{\Lambda\Lambda}$Ne, ${}^{26}_{\Lambda\Lambda}$Mg, ${}^{30}_{\Lambda\Lambda}$Si, ${}^{34}_{\Lambda\Lambda}$S, ${}^{38}_{\Lambda\Lambda}$Ar, ${}^{42}_{\Lambda\Lambda}$Ca, ${}^{92}_{\Lambda\Lambda}$Zr and ${}^{142}_{\Lambda\Lambda}$Ce, ${}^{210}_{\Lambda\Lambda}$Pb are shown in Table 3. The empirical Λ binding energy B_Λ of Table 3 has been calculated using the empirical formula

$$B_\Lambda(A) = [(27.0 - 81.9\ A^{-2/3}) \pm 1.5]\ \mathrm{MeV} \tag{33}$$

where A is the mass number of the single-Λ hypernuclei [9]. The calculated binding energy, $B_{\Lambda\Lambda}$, of ${}^{6}_{\Lambda\Lambda}$He agrees fairly well with the experimental value 10.90±0.50 MeV [2] within the experimental error limit. But that for ${}^{10}_{\Lambda\Lambda}$Be is slightly larger than the

Table 3. The calculated Λ binding energy (B_Λ), two-Λ separation energy ($B_{\Lambda\Lambda}$) and the ΛΛ bond energy ($\Delta B_{\Lambda\Lambda}$) for different Λ- and double-Λ hypernuclei.

Hyper-nuclei	B_Λ (MeV)	Hyper-nuclei	$B_{\Lambda\Lambda}$ (MeV)	$\Delta B_{\Lambda\Lambda}$ (MeV)	$\Delta B^{\mathrm{Expt}}_{\Lambda\Lambda}$ (MeV)
${}^{5}_{\Lambda}$He	3.1214	${}^{6}_{\Lambda\Lambda}$He	10.8936	4.6508	4.7 ± 0.60 [2]
${}^{9}_{\Lambda}$Be	6.7136	${}^{10}_{\Lambda\Lambda}$Be	18.8567	5.4295	4.3 ± 0.40 [1]
${}^{13}_{\Lambda}$C	11.2226	${}^{14}_{\Lambda\Lambda}$C	28.4294	5.9842	-
${}^{17}_{\Lambda}$O	14.6000	${}^{18}_{\Lambda\Lambda}$O	35.3013	6.1013	-
${}^{21}_{\Lambda}$Ne	16.2401	${}^{22}_{\Lambda\Lambda}$Ne	38.4235	5.9433	-
${}^{25}_{\Lambda}$Mg	17.4237	${}^{26}_{\Lambda\Lambda}$Mg	40.5915	5.7441	-
${}^{29}_{\Lambda}$Si	18.3322	${}^{30}_{\Lambda\Lambda}$Si	42.1986	5.5342	-
${}^{33}_{\Lambda}$S	19.0440	${}^{34}_{\Lambda\Lambda}$S	43.4290	5.3410	-
${}^{37}_{\Lambda}$Ar	19.6224	${}^{38}_{\Lambda\Lambda}$Ar	44.4146	5.9547	-
${}^{41}_{\Lambda}$Ca	20.1158	${}^{42}_{\Lambda\Lambda}$Ca	45.1995	4.9679	-
${}^{91}_{\Lambda}$Zr	22.1668	${}^{92}_{\Lambda\Lambda}$Zr	47.7106	3.3770	-
${}^{141}_{\Lambda}$Ce	24.5028	${}^{142}_{\Lambda\Lambda}$Ce	51.6452	2.6446	-
${}^{209}_{\Lambda}$Pb	26.3107	${}^{210}_{\Lambda\Lambda}$Pb	54.9813	2.3599	-

experimental value 17.7 ± 0.40 MeV [1]. The ΛΛ, ΛN effective, Λ-core folded and (ΛΛ)-core effective three-body potentials for ${}^{6}_{\Lambda\Lambda}$He hypernucleus are shown in Fig. 3 as a representative case. The variation of the two-Λ separation energy with mass number A for $A_c \leq 40$ is displayed in Fig. 4 and the same for mass number $A_c \geq 40$ is shown in Fig. 5. The two-Λ separation energy $B_{\Lambda\Lambda}$ shows saturation in the heavy-mass region. Having obtained the wave function by the HHE approach, some of the observables of the three-body system have been calculated. These include the root mean square (r.m.s.) radius of the three-body system

$$R_A = \left[\frac{A_c R_c^2 + m_\Lambda < r_{13}^2 + r_{12}^2 >}{A_c + 2m_\Lambda}\right]^{1/2}, \tag{34}$$

whereA_c, m_Λ are the masses of the core and the Λ-hyperon (in units of the nucleon mass) and R_c is the matter radius of the core determined by the relation

$R_c = r_0 A_c^{1/3}$ with $r_0 = 1.1$ fm. The r.m.s. core–Λ separation is defined as

$$R_{c\Lambda} = \left[< r_{13}^2 + r_{12}^2 > /2\right]^{1/2}. \tag{35}$$

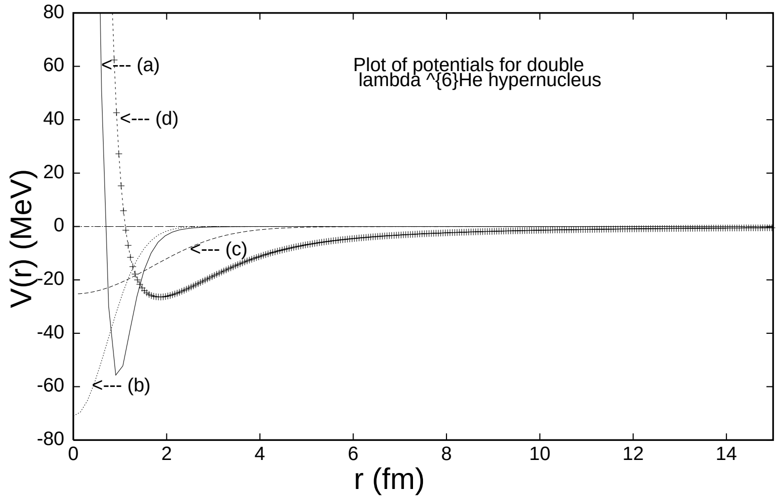

Fig. 3. Plot of the ΛΛ, ΛN and effective core–Λ potentials for ${}^{6}_{\Lambda\Lambda}$He. *(a) ΛΛ potential, (b) ΛN effective potential, (c) core–Λ folded potential and (d) (ΛΛ)–core three-body effective potential. For graphs (a)-(b), r is the relative separation and for (d) it is the hyper-radial separation in the same scale.*

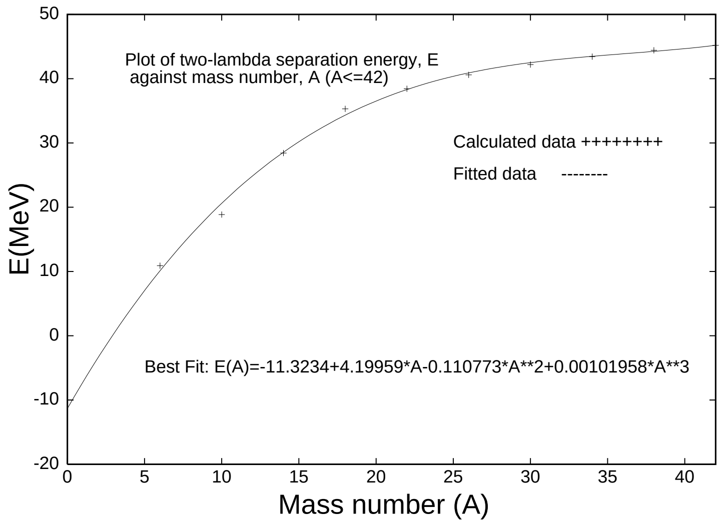

Fig. 4. Plot of the two-Λ binding energy $B_{\Lambda\Lambda}$ against mass A ($A \leq 42$) of the double-Λ hypernuclei. (Data taken from Table 3.)

The expectation value of the observables $< r_{13}^2 + r_{12}^2 >$ is obtained by the expression

$$< r_{13}^2 + r_{12}^2 >= \sum_{KK'l_{x_1}LS} \int_0^\infty \rho^2 \mathrm{d}\rho U_{Kl_{x_1}LS}(\rho) U_{K'l_{x_1}LS}(\rho)$$
$$\int_0^{\pi/2} {}^{(2)}P_K{}^{l_{x_1},l_{x_1}}(\phi)\, {}^{(2)}P_{K'}{}^{l_{x_1},l_{x_1}}(\phi) \left[\frac{1}{2a_{23}^2} \cos^2\phi + \frac{2}{a_{(23)1}^2} \sin^2\phi\right] \cos^2\phi \sin^2\phi \,\mathrm{d}\phi. \tag{36}$$

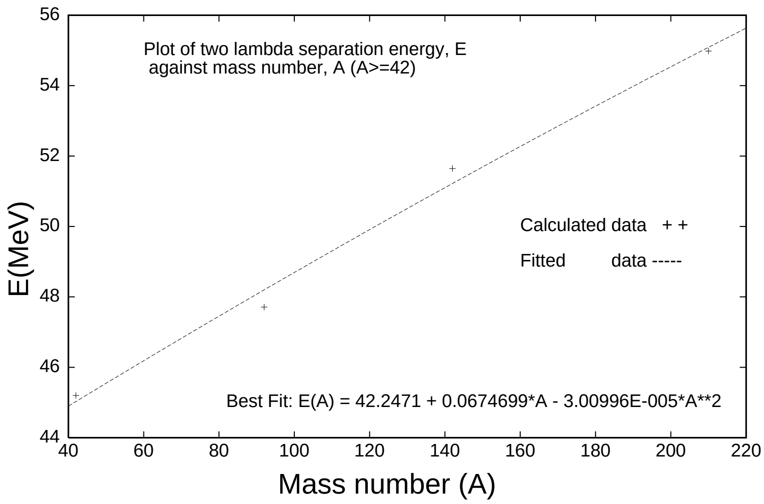

Fig. 5. Plot of the two-Λ binding energy $B_{\Lambda\Lambda}$ against mass A (A≥ 42) of the double-Λ hypernuclei. (Data taken from Table 3.)

The r.m.s. separation between the valence Λ-hyperons ($R_{\Lambda\Lambda}$) is given by the expression

$$R_{\Lambda\Lambda} = \left[< r_{23}^2 >\right]^{1/2}, \tag{37}$$

where

$$\begin{aligned} < r_{23}^2 > &= \frac{1}{a_{23}^2} \sum_{KK'l_{x_1}LS} \int_0^\infty \rho^2 \mathrm{d}\rho U_{Kl_{x_1}LS}(\rho) U_{K'l_{x_1}LS}(\rho) \\ &\times \int_0^{\pi/2} {}^{(2)}P_K{}^{l_{x_1},l_{x_1}}(\phi)\, {}^{(2)}P_{K'}{}^{l_{x_1},l_{x_1}}(\phi)\, \cos^4\phi\, \sin^2\phi \,\mathrm{d}\phi. \end{aligned} \tag{38}$$

The r.m.s. separation between the core (^{4}He, ^{8}Be, ^{12}C etc.) and the C.M. of ΛΛ pair is given by the expression

$$R_{(\Lambda\Lambda)c} =< r_{(23)1}^2 >^{1/2}, \tag{39}$$

where

$$< r^2_{(23)1} > \; = \; \frac{1}{a^2_{(23)1}} \sum_{KK'l_{x_1}LS} \int_0^\infty \rho^2 \mathrm{d}\rho U_{Kl_{x_1}LS}(\rho) U_{K'l_{x_1}LS}(\rho) \times \int_0^{\pi/2} {}^{(2)}P_K{}^{l_{x_1},l_{x_1}}(\phi)\; {}^{(2)}P_{K'}{}^{l_{x_1},l_{x_1}}(\phi)\; \cos^2\phi\; \sin^4\phi \mathrm{d}\phi. \tag{40}$$

The computed value of these r.m.s. radii are listed in Tables 4, 5 and 6. Finally, we computed the correlation coefficient defined as

$$\eta = < \frac{r^2_{(\Lambda\Lambda)c}}{\rho^2} > = \frac{1}{a^2_{(23)1}} \sum_{KK'l_{x_1}LS} \int_0^\infty \mathrm{d}\rho U_{Kl_{x_1}LS}(\rho) U_{K'l_{x_1}LS}(\rho) \times \int_0^{\pi/2} {}^{(2)}P_K{}^{l_{x_1},l_{x_1}}(\phi) {}^{(2)}P_{K'}{}^{l_{x_1},l_{x_1}}(\phi) \cos^2\phi \sin^4\phi \mathrm{d}\phi. \tag{41}$$

A small value of this coefficient will indicate that the two valence Λ-hyperons are situated on two opposite sides of the α–core (i.e., a cigar shape where the Λ-hyperons are anti-correlated). A large value (≤ 1) will indicate the possibility of $\Lambda - \Lambda$ correlation.

Table 4. Calculated BE $B_{\Lambda\Lambda}$ and r.m.s. radii for different $K_{\max}$ for ${}^{6}_{\Lambda\Lambda}$He hypernucleus.

$K_{\max}$	BE	r.m.s. radii (fm)						η
	(MeV)	R_A	$R_{c\Lambda}$	$R_{\Lambda\Lambda}$	$R_{(\Lambda\Lambda)c}$	R_c^{CM}	R_Λ^{CM}	
0	09.09925	2.0747	2.5327	3.1446	1.9856	0.7405	2.0056	0.3157
2	09.41083	2.0535	2.4860	3.1220	1.9348	0.7216	1.9770	0.3158
4	09.85415	2.0507	2.4798	3.0914	1.9391	0.7232	1.9666	0.3187
6	10.16209	2.0360	2.4472	3.0466	1.9153	0.7143	1.9398	0.3209
8	10.41431	2.0262	2.4251	3.0065	1.9030	0.7097	1.9193	0.3237
10	10.59790	2.0208	2.4131	2.9791	1.8985	0.7080	1.9068	0.3263
12	10.72117	2.0187	2.4085	2.9612	1.8996	0.7085	1.9003	0.3285
14	10.79954	2.0185	2.4079	2.9497	1.9034	0.7099	1.8973	0.3302
16	10.85764	2.0191	2.4092	2.9422	1.9079	0.7116	1.8962	0.3315
18	10.87652	2.0199	2.4111	2.9373	1.9122	0.7132	1.8959	0.3323
20	10.89363	2.0207	2.4129	2.9340	1.9158	0.7145	1.8961	0.3329

Table 5. Calculated BE $B_{\Lambda\Lambda}$ and r.m.s. radii for different $K_{\max}$ for $^{10}_{\Lambda\Lambda}$Be hypernucleus.

$K_{\max}$	BE (MeV)	r.m.s. radii (fm)						η
		R_A	$R_{c\Lambda}$	$R_{\Lambda\Lambda}$	$R_{(\Lambda\Lambda)c}$	R_c^{CM}	R_Λ^{CM}	
0	16.85281	2.2092	2.2399	2.9556	1.6833	0.3858	1.9665	0.2848
2	17.24068	2.2030	2.2129	2.8655	1.6865	0.3866	1.9345	0.2955
4	17.65940	2.2007	2.2030	2.8394	1.6845	0.3861	1.9239	0.2975
6	18.00125	2.1951	2.1787	2.8016	1.6687	0.3825	1.9017	0.2997
8	18.29194	2.1916	2.1631	2.7698	1.6616	0.3809	1.8863	0.3024
10	18.50776	2.1899	2.1555	2.7468	1.6613	0.3808	1.8777	0.3050
12	18.65403	2.1894	2.1532	2.7308	1.6649	0.3816	1.8738	0.3072
14	18.74717	2.1895	2.1536	2.7198	1.6700	0.3828	1.8725	0.3089
16	18.80392	2.1898	2.1552	2.7124	1.6750	0.3839	1.8724	0.3102
18	18.83741	2.1902	2.1569	2.7073	1.6792	0.3849	1.8729	0.3110
20	18.85670	2.1905	2.1584	2.7039	1.6825	0.3857	1.8734	0.3116

Table 6. The r.m.s. matter radii and correlation coefficient for different double-Λ hypernuclei at $K_{\max} = 20$.

Hypernuclei	r.m.s. radii (fm)						η
	R_A	$R_{c\Lambda}$	$R_{\Lambda\Lambda}$	$R_{(\Lambda\Lambda)c}$	R_c^{CM}	R_Λ^{CM}	
$^{6}_{\Lambda\Lambda}$He	2.0207	2.4129	2.9340	1.9158	0.7145	1.8961	0.3329
$^{10}_{\Lambda\Lambda}$Be	2.1905	2.1584	2.7035	1.6825	0.3857	1.8734	0.3116
$^{14}_{\Lambda\Lambda}$C	2.4441	2.0281	2.5638	1.5716	0.2600	1.8340	0.3034
$^{18}_{\Lambda\Lambda}$O	2.6841	1.9966	2.5321	1.5438	0.1998	1.8464	0.3000
$^{22}_{\Lambda\Lambda}$Ne	2.8984	2.0191	2.5623	1.5601	0.1659	1.8938	0.2989
$^{26}_{\Lambda\Lambda}$Mg	3.0883	2.0477	2.5970	1.5833	0.1428	1.9394	0.2985
$^{30}_{\Lambda\Lambda}$Si	3.2593	2.0827	2.6421	1.6102	0.1261	1.9869	0.2982
$^{34}_{\Lambda\Lambda}$S	3.4150	2.1170	2.6808	1.6386	0.1134	2.0305	0.2985
$^{38}_{\Lambda\Lambda}$Ar	3.5583	2.1510	2.7211	1.6660	0.1033	2.0720	0.2988
$^{42}_{\Lambda\Lambda}$Ca	3.6912	2.1814	2.7558	1.6911	0.0949	2.1086	0.2990
$^{92}_{\Lambda\Lambda}$Zr	4.8833	2.5839	3.2502	2.0089	0.0517	2.5439	0.3014
$^{142}_{\Lambda\Lambda}$Ce	5.6759	2.8676	3.6100	2.2283	0.0372	2.8388	0.3017
$^{210}_{\Lambda\Lambda}$Pb	6.4898	3.2602	4.1418	2.5179	0.0285	3.2382	0.3008

The computed values of this coefficient for various three-body systems are shown in the last column of Tables 4, 5 and 6. As the value of η is small (≈ 0.30), a cigar shape is indicated on the average.

4. *Summary and conclusion*

Since hyperons and nucleons have three-quark (qqq) structures (e.g. p$\rightarrow$ uud, n$\rightarrow$ udd, $\Lambda^0 \rightarrow$ uds etc.), interactions among them as well as with nucleons should give important inputs in the knowledge of strong interactions. But not much attention has so far been directed to the study of hyperon-hyperon and hyperon-nucleon interaction through the investigation of hypernuclei. We have undertaken a systematic study of the bound-state properties of hypernuclei to shed light on the hyperon-hyperon and hyperon-nucleon interactions. The hyperspherical harmonics expansion (HHE) method adopted here is an essentially exact method, where calculations can be carried out up to any desired precision by gradually increasing the expansion basis. This can be seen in the first two columns of Tables 4 and 5 where the binding energies gradually attain a convergence with increasing $K_{\max}$ values. It is also found from Tables 4 and 5 that the convergence in the binding energy (with respect to increasing $K_{\max}$) is relatively slow, whereas the convergence rates for the other observables are faster. For ${}^{6}_{\Lambda\Lambda}$He, the calculated two-Λ separation energy $B_{\Lambda\Lambda}$ at $K_{\max} = 20$ (see Table 4) and $\Lambda\Lambda$ bond energy $\Delta B_{\Lambda\Lambda}$ (see Table 3) agrees fairly well with the experimental values 10.90 ± 0.50 MeV [2] and 4.70 ± 0.60 MeV, respectively, and our previous calculation [70] within the allowed error limit. However, the calculated $B_{\Lambda\Lambda}$ at $K_{\max} = 20$ (see Table 5) and $\Delta B_{\Lambda\Lambda}$ (see Table 3) for ${}^{10}_{\Lambda\Lambda}$Be are slightly greater than the experimental values 17.70 ± 0.40 MeV [1] and 4.30 ± 0.40 MeV [1], respectively. The convergence in the HH expansion is not fully attained with $K_{\max} = 20$, but we do not need higher precision at this stage of the game, because input data are not that accurate. As discussed earlier, the strength of the ΛN effective potential decreases as the mass (A_c) of the core nuclei increases (see Table 2). In the mass region $A_c \leq 40$, the ΛN potential strength falls rapidly, while it falls relatively slowly in the mass region $30 \leq A_c \leq 140$ and reaches saturation beyond that. Studying the trend of the variation of the ΛN effective potential with the mass of the core (see Fig. 2) we fitted the empirical relation

$$V_0(A_c) = [12.7458 \quad \log_e(A_c) - 84.1403] \text{ MeV} \tag{42}$$

for $A_c \leq 40$. The calculated two-Λ separation energy, $B_{\Lambda\Lambda}$, shows the saturation property in the heavy-mass region and a relatively faster rise in the low-mass region. Studying the nature of the variation of the calculated $B_{\Lambda\Lambda}$ with the mass (A) of the double-Λ hypernuclear systems (see Figs. 4 and 5), we fitted the following empirical formula for the two-Λ separation energy $B_{\Lambda\Lambda}$

$$\begin{aligned} B_{\Lambda\Lambda}(A) &= (a_0 + a_1 A + a_2 A^2 + a_3 A^3) \text{ MeV} \quad \text{for } A_c \leq 40 \\ &= (b_0 + b_1 A + b_2 A^2) \text{ MeV} \quad \text{for } A_c \geq 40 \end{aligned} \tag{43}$$

with $a_0 = -11.3234, a_1 = 4.19959, a_2 = -0.110773, a_3 = 0.00101958, b_0 = 42.2471,$ $b_1 = 0.0674699$and $b_2 = -3.00996 \times 10^{-5}$. A relatively small value (≈ 0.32) (see Tables 4, 5 and 6) of the calculated correlation coefficient indicates that the valence hyperons are not correlated.

Thus, we conclude that the effective ΛN interaction (between a nucleaon embedded in the core and a valence Λ) can be represented by a single term attractive Gaussian, whose strength decreases with increasing core mass (A_c). A smooth dependence on A_c over the entire mass range has been found. The gradual decrease in the strength may be viewed as the effect of screening of the interacting nucleon embedded in the core, by the surrounding nucleons. One intuitively expects such a result. As A_c increases, the valence Λ particles are gradually surrounded by other nucleons and effective ΛN interaction attains it saturation value.

Acknowledgement

Part of the calculation was done on computers provided by the Departmental Special Assistance (DSA) of the University Grants Commission (UGC), India.

References

[1] M. Danysz et al., Nucl. Phys. **49** (1963) 121.

[2] D. J. Prowse, Phys. Rev. Lett. **17** (1966) 782.

[3] R. H. Dalitz, D. H. Davis, P. H. Fowler, A. Montwill, J. Poriewski and J. A. Zakrzewski, Proc. R. Soc. (London), Ser. **A426** (1989) 1.

[4] S. Aoki et al., Prog. Theor. Phys. **85** (1991) 1287.

[5] H. Nemura et al., Prog. Theor. Phys. **85** (2000) 929.

[6] J. Caro et al., Nucl. Phys. **A646** (1999) 299.

[7] Y. Yamamoto et al., Nucl. Phys. **A547** (1992) 233c.

[8] H. Himeno et al., Prog. Theor. Phys. **89** (1993) 109.

[9] A. Gal, Adv. Nucl. Phys., eds. M. Baranger and E. Vogt. Vol. **8**, Plenum (1975) p.1.

[10] G. Alexander et al., Phys. Rev. **173** (1968) 1452.

[11] B. Sechi - Zorn et al., Phys. Rev. **175** (1968) 1735.

[12] J. A. Kadyk et al., Nucl. Phys. **B27** (1971) 13.

[13] J. M. Hauptman, LBL Report No. LBL-3608 (1974).

[14] F. Eisele et al., Phys. Lett. B **37** (1971) 204.

[15] R. Engelmann et al., Phys. Lett. **21** (1966) 487.

[16] Y. C. Tang and R. C. Herndon, Nuovo Cimento B **46** (1966) 117.

[17] R. H. Dalitz and G. Rajasekaran, Nucl. Phys. **50** (1964) 450.

[18] A. R. Ali and A. R. Bodmer, Phys. Lett. **24B** (1967) 343.

[19] A. R. Bodmer, Q. N. Usmani and J. Carlson, Nucl. Phys. A **422** (1984) 510.

[20] K. Ikeda, H. Bando and T. Motoba, Prog. Theor. Phys., Suppl. no. **81** (1985) 147.

[21] C. D. Lin, Phys. Rep. **257** (1995) 1.

[22] T. H. Gronwall, Phys. Rev. **51** (1937) 655.

[23] C. D. Lin, Phys. Rev. A **29** (1984) 1019.

[24] C. D. Lin, Phys. Rev. Lett. **51** (1983) 1348.

[25] J. Macek, J. Phys. B **1** (1968) 831.

[26] C. H. Greene, Phys. Rev. A **23** (1981) 661.

[27] C. D. Lin, Xian-Hui Liu, Phys. Rev. A **37** (1988) 2749.

[28] H. Fakuda, T. Ishihura and S. Hara, Phys. Rev. A **41** (1990) 1455.

[29] A. M. Launay and M. Le Dourneuf, J. Phys. B **15** (1982) 455.

[30] J. L. Ballot and J. Navarro, J. Phys. B **8** (1975) 172.

[31] R. C. Whitten and J. S. Sims, Phys. Rev. A **9** (1974) 1586.

[32] R. M. Shoucri and B. T. Darling, Phys. Rev. A **12** (1975) 2272.

[33] V. B. Mandelzweig, Phys. Lett. A **78** (1980) 25.

[34] V. D. Efros, A. M. Frolov and M. I. Mukhtarova, J. Phys. B **15** (1982) 1819.

[35] T. K. Das, R. Chattopadhyay and P. K. Mukherjee, Phys. Rev. A **A50** (1994) 3521.

[36] R. Chattopadhyay, T. K. Das and P. K. Mukherjee, Phys. Scripta **54** (1996) 601.

[37] R. Chattopadhyay and T. K. Das, Phys. Rev. A **57** (1997) 1281.

[38] Md. A. Khan, S. K. Datta, and T. K. Das, Fizika B (Zagreb) **8** (1999) 469.

[39] T. K. Das, H. T. Coelho and M. Fabre de la Ripelle, Phys. Rev. C **26** (1982) 2288.

[40] H. T. Coelho, T. K. Das and M. Fabre de la Ripelle, Phys. Letts. B **109** (1982) 255.

[41] T. K. Das and H. T. Coelho, Phys. Rev. **C26** (1982) R754.

[42] S. Bhattacharya, T. K. Das, K. P. Kanta and A. K. Ghosh, Phys. Rev. C **50** (1994) 2228.

[43] Khan M. A., Dutta S. K., Das T. K. and Pal M. K., J. Phys. G: Nucl. Part. Phys. **24** (1998) 1519.

[44] Yu. A. Simonov, Yad. Fiz. **3** (1960) 630 [Sov. J. Nucl. Phys. **3** (1960) 461]; in *Proc. Int. Symp. on the Present Status and Novel Developments in the Nuclear Many Body Problem*, Rome, 1972, eds. F. Calogena and C. Ciofi Degli Atti, Editrice composition, Bologna (1973) p.527; Sov. J. Nucl. Phys. **7** (1968) 722.

[45] F. Zernike and H. C. Brinkman, Proc. Kon. Acad. Wtensch, **33** (1975) 3.

[46] M. Fabre de la Ripelle, *Proc. Int. School Nucl. Theo. Phys.*, Predeal (1969).

[47] M. Fabre de la Ripelle, Comp. Rendu. Acad. Sci. (Paris) B **269** (1970) 80; A **273** (1971) 1007.

[48] G. Erens, J. L. Visschers and R. Van Wageningen, Ann. Phys. **67** (1971) 461.

[49] J. L. Ballot, Z. Phys. A **302** (1981) 347; Few Body Systems (Austria), Suppl. **1** (1986) 146.

[50] J. L. Ballot and M. Fabre de la Ripelle, Ann. Phys. (N. Y.) **127** (1980) 62.

[51] J. M. Richard, Phys. Rep. **212** (1992) 1.

[52] H. Leeb, H. Fiedeldey, E. G. O. Gavin, S. A. Sofianos and R. Lipperheide, Few Body Systems (Austria) **12** (1992) 55.

[53] N. Barnea and A. Novoselsky, Ann. Phys. (N. Y.) **256** (1997) 192.

[54] S. Watanabe, Y. Hosoda and D. Kato, J. Phys. **B26** (1993) L495.

[55] B. R. Johnson, J. Chem. Phys. **69** (1978) 4678.

[56] A. K. Ghosh and T. K. Das, Fizika (Zagreb) **22** (1990) 521.

[57] M. Abramoitz and I. A. Stegun, *Handbook of Mathematical Functions*, Dover Publications, NY (ninth printing), p. 774.

[58] J. Raynal and J. Revai, Nuovo Cimento **68** (1970) 612.

[59] T. B. De and T. K. Das, Phys. Rev. C **36** (1987) 402.

[60] T. K. Das, H. T. Coelho and M. Fabre de la Ripelle, Phys. Rev. C **26** (1982) 2281.

[61] Y. Yamamoto and H. Bando, Prog. Theor. Phys., Suppl. **81** (1985) 9.

[62] Y. Yamamoto, T. Motoba, H. Himeno, K. Ikeda and S. Nagata, Prog. Theor. Phys., Suppl. **117** (1994) 361.

[63] M. M. Nagets, T. A. Rijken and J. J. deSwart, Phys. Rev D **15** (1977) 547; **20** (1979) 1633.

[64] R. H. Dalitz, Phys. Rev. **112** (1958) 605.

[65] R. H. Dalitz and L. Liu, Phys. Rev **116** (1959) 1312.

[66] M. M. Block and R. H. Dalitz, Phys. Rev. Lett. **11** (1963) 96.

[67] J. B. Adams, Phys. Rev. **156** (1967) 1611.

[68] C. Y. Chung, D. P. Heddle and L. S. Kisslinger, Phys. Rev. C **27** (1983) 335.

[69] B. H. Mc Kellar and B. F. Gibson, *Proc. Int. Conf. on Hypernuclear and Kaon Physics*, Heidelberg, 1982, ed. B. Povh, p.156; Phys. Rev. C **30** (1984) 322.

[70] Md. A. Khan and T. K. Das, Fizika B (Zagreb) **9** (2000) 55.

[71] M. May et al., Phys. Rev. Lett. **47** (1981) 1106.

ISTRAŽIVANJE DINAMIKE $\Lambda\Lambda$ I EFEKTIVNOG MEĐUDJELOVANJA ΛN U HIPERJEZGRAMA MALE I SREDNJE MASE

Pažljivo razmatramo dinamiku $\Lambda\Lambda$ istraživanjem fenomenoloških potencijala $\Lambda\Lambda$ i Λ-nukleon proučavanjem vezanih stanja hiperjezgri s dvije Λ čestice ${}^{6}_{\Lambda\Lambda}$He, ${}^{10}_{\Lambda\Lambda}$Be, ${}^{14}_{\Lambda\Lambda}$C, ${}^{18}_{\Lambda\Lambda}$O, ${}^{22}_{\Lambda\Lambda}$Ne, ${}^{26}_{\Lambda\Lambda}$Mg, ${}^{30}_{\Lambda\Lambda}$Si, ${}^{34}_{\Lambda\Lambda}$S, ${}^{38}_{\Lambda\Lambda}$Ar, ${}^{42}_{\Lambda\Lambda}$Ca, ${}^{92}_{\Lambda\Lambda}$Zr i ${}^{142}_{\Lambda\Lambda}$Ce, ${}^{210}_{\Lambda\Lambda}$Pb u okviru modela tri čestice (sredica+Λ+Λ). Djelotvoran potencijal ΛN smo dobili ugradnjom fenomenološkog potencijala ΛN u prostornu raspodjelu nukleona u sredici. Ponovili smo ranija dva računa, (tj., ${}^{6}_{\Lambda\Lambda}$He i ${}^{10}_{\Lambda\Lambda}$Be) da bismo opravdali ispravnost ovog modela potencijala. Uz pretpostavku tog modela potencijala, predvidjeli smo strukturu težih hiperjezgri s dvije Λ čestice. U tim razmatranjima sustava tri tijela primijenili smo razvoj po hipersfernim harmonicima, što je u biti egzaktna metoda. Postigli smo konvergenciju točnosti 0.25% za $K_{\max} = 20$. U ovim računima nisu primijenjena približenja koja bi ograničavala dozvoljene vrijednosti l parova čestica koje međudjeluju.